Electronic Supplementary Information

From Centrosymmetric to Noncentrosymmetric: Intriguing Structure Evolution in d^{10}-transition Metal Iodate Fluorides

Liling Cao,[abc] Min Luo,*[ac] Chensheng Lin,[d] Yuqiao Zhou,[e] Dan Zhao,[f] Tao Yan,[ac] Ning Ye,*[ac]

[a]Key Laboratory of Optoelectronic Materials Chemistry and Physics, Fujian Institute of Research on the Structure of Matter, Chinese Academy of Sciences, Fuzhou, Fujian 350002, China.
[b]University of the Chinese Academy of Sciences, Beijing 100049, China.
[c]Fujian Science & Technology Innovation Laboratory for Optoelectronic Information of China, Fuzhou, Fujian 350002, China.
[d]State Key Laboratory of Structural Chemistry, Fujian Institute of Research on the Structure of Matter, Chinese Academy of Science, Fuzhou, Fujian 350002, China.
[e]Key Laboratory of Green Chemistry and Technology, Ministry of Education, College of Chemistry, Sichuan University, Chengdu 610064, China.
[f]College of Chemistry and Chemical Engineering, Henan Polytechnic University, Jiaozuo, Henan 454000, China.

E-mail: nye@fjirsm.ac.cn

Experimental Section

Reagents.

$Cd(OH)_2$ (98.5%, aladdin), $Zn(NO_3)_2.6H_2O$(99%+, adamas), CdF_2 (98%+, adamas), ZnF_2 (99%, adamas), HIO_3 (99.5%, macklin). All of the chemicals were of analytical grade from commercial sources and used as received.

Synthesis.

Single crystals of MIO_3F (M = Zn, Cd) were synthesized with a facile hydrothermal method.[1] The mixture of $Zn(NO_3)_2.6H_2O$ (0.706 g, 3mmol), ZnF_2 (0.517 g, 5mmol), HIO_3 (1.407 g, 8 mmol) in H_2O (8 mL) was sealed in an autoclave with a Teflon liner (23 mL) and heated at 240 ^oC for 5 days, which was then slowly cooled to room temperature at a rate of 3 ^oC/h. The mixture of $Cd(OH)_2$ (1.147 g, 8 mmol), CdF_2 (0.752 g, 5mmol), HIO_3 (1.759 g, 10 mmol) in H_2O (8 mL) was sealed in an autoclave with a Teflon liner (23 mL) and heated at 270 ^oC for 5 days, which was then slowly cooled to room temperature at a rate of 3 ^oC/h. The reaction products were washed with deionized water and ethanol and then dried in the air. The reaction product was colorless, transparent, and nonhygroscopic single crystals.

Single-Crystal Structure Determination.

Single crystal X-ray diffraction intensities of both $ZnIO_3F$ and $CdIO_3F$ were obtained on a Bruker D8 Venture equipped with Photon II CMOS detector and a micro-focus Mo radiation source (λ = 0.71073 Å). The data sets were collected at 140(2) K by ω and φ scans with a frame width of 0.5° and corrected by face-indexed numerical absorptions with transmission factors of 0.195 – 0.262 for $ZnIO_3F$ calculated by *SADABS* (version 2016/2) and 0.294916 – 0.432999 for $CdIO_3F$ calculated by *TWINABS* (version 2012/1), respectively. Structure solutions were solved by SHELXT (version 2014/5) and refinements were processed with the use of SHELXL (version 2018/1).

The crystal of $CdIO_3F$ was found to display non-merohedral twinning. The program *CELL_NOW* (version 2008/4) indexed two components with the second twin component related to the first one by 86.6° about the [1.000 0.267 0.277] axis in real space and about the [0.911 0.263 1.000] the reciprocal space. The reflections were integrated and written into a HKLF5 file. All programs listed in the structure determination were supplied by Bruker AXS Inc., Madison, WI, 2014. For both $ZnIO_3F$ and $CdIO_3F$, Laue symmetry and systematic absences led to the monoclinic space group $P2_1/n$ and orthorhombic space group $P2_12_12_1$, respectively. All atoms were atoms were refined with anisotropic displacement parameters and results in good agreement factors with $R(F_o^2 > 2\sigma(F_o^2))$ of 0.0229 and 0.0272, respectively. The large residual intensities of $CdIO_3F$ on the Fourier electron difference maps may be attributed to the cut-off effect when the IAM refinements were applied. Specifically, the positive peak may be assigned to lone-pair electrons of I atom. *ADDSYM* implemented in *PLATON* were carries out and no higher symmetry were found in the structures. Relevant crystallographic data and details of the experimental conditions are summarized in Table S1. Atomic coordinates and isotropic displacement coefficients are listed in Tables S2 – S3 and bond lengths and angles in Tables S4 – S5.

Powder X-ray Diffraction (XRD).

X-ray diffraction patterns for polycrystalline materials were collected on a Mini-flex-600 powder X-ray diffractometer by using Cu Kα radiation (λ = 1.54059 Å) at room temperature in the angular range of 2θ = 5−85° with a scan step width of 0.02° and a fixed time of 0.2 s. The powder XRD patterns for the pure powder samples are in very good agreement with the calculated XRD patterns (using PCWEXE) from the single-crystal models) (Figure S1).

Energy-dispersive X-ray Spectroscopy Analysis.

Microprobe elemental analyses were performed on a field emission scanning electron microscope (FESEM, SU-8010) equipped with an energy dispersive X-ray spectrometer (EDS) (Figure S2).

Thermal Analysis.

The thermogravimetric analyses (TGA) were performed on a NETZSCH STA449F3 simultaneous analyzer. Reference (Al_2O_3) and crystal samples (5-10 mg) were enclosed in Al_2O_3 crucibles and heated from 30 to 1300 ^oC at a rate of 10 $^oC \cdot min^{-1}$ under a constant flow of nitrogen gas (Figure S3).

UV-vis diffuse Reflectance Spectroscopy.

UV-vis diffuse reflectance spectra were recorded at room temperature using a powder sample with $BaSO_4$ as a standard (100% reflectance) on a PerkinElmer Lamda-950 UV/vis/NIR spectrophotometer over the scan range 200-2500 nm. Reflectance values were converted to absorbance using the Kubelka-Munk function.[4]

Birefringence.

The birefringences of MIO_3F (M = Zn, Cd) were measured by the polarizing microscope equipped (ZEISS Axio Scope. A1) with Berek compensator. The wavelength of monochromatic light is 546.1 nm. The boundary lines of the first, second and third order interference color are relatively clear, the relative error is smaller. Therefore, in order to improve the test accuracy, the samples to be screened should be clean and transparent lamellar crystals. The formula for calculating birefringence is listed below,

$$R=(|N_e-N_o|)\times T=\Delta n\times T \quad (1)$$

R denotes retardation, Δn represents birefringence, and T means the thickness of crystal. According to Eq. (1), the birefringence can be got.

Infrared (IR) Spectroscopy.

The Fourier transform infrared spectroscopy (FTIR) spectra (KBr pellet) were recorded on a Bruker VERTEX 70 Fourier spectrometer in the 4000-400 cm^{-1} range.

Second-harmonic Generation (SHG).

Polycrystalline SHG signals were measured by Kurtz-Perry method.[5] The measurements were made on a Q-switched Nd : YAG solid-state laser of wavelength 1064 nm. SHG efficiencies have significant correlation with the following particle size ranges: 25-45, 45-62, 62-75, 75-109, 109-150, and 150-212 μm. The samples of different particle sizes were pressed between two rounded 1 mm thick sheet glasses with a 2 mm thick rubber ring interlayer containing an 8 mm diameter hole in the middle, which were tightly sheathed in an aluminous round box with an 8 mm diameter hole in the middle. The KDP (KH_2PO_4) used as the references was also ground and sieved into the same particle size ranges. A cutoff filter was used to limit background flash-lamp light on the sample, and an interference filter (530 ± 10 nm)

was used to select the second harmonic for detection with a photomultiplier tube attached to a RIGOL DS1052E 50 MHz oscilloscope. The ratio of the second-harmonic intensity outputs was calculated. No index-matching fluid was used in any of the experiments.

Electronic Structure Calculations.

The electronic structure for MIO_3F (M = Zn, Cd) were investigated by using density functional theory (DFT) [6] calculation with CASTEP [7] code provided by the Material Studio package. Generalized gradient approximation (GGA) [8] in the scheme of Perdew-Burke-Emzerhoff (PBE) was adopted to describe the exchange-correlation energy. The optimized norm-conserving pseudopotentials in the Kleinman-Bylander [9] form for all the elements were used to model the effective interaction between atom cores and valence electrons. Cd $4d^{10}5s^2$, Zn $3d^{10}4s^2$, I $5s^25p^5$, O $2s^22p^4$ and F $2s^22p^5$ electrons were treated as valence electrons, allowing the adoption of a relatively small basis set without compromising the computational accuracy. The k-point of first Brillouin zones for crystals MIO_3F (M = Zn, Cd) were sampled as 3×3×1 and 3×2×1 Monkhorst-Pack scheme. The high kinetic energy cutoff was set to be 850eV and 850 eV.

Table S1. Crystal data and structure refinement for MIO_3F (M = Zn, Cd).

Formula	$ZnIO_3F$	$CdIO_3F$
Formula Mass(amu)	259.27	306.30
Crystal System	monoclinic	orthorhombic
Space Group	$P2_1/c$	$P2_12_12_1$
a(Å)	5.0197(4)	5.5051(4)
b (Å)	5.2136(4)	5.7913(4)
c (Å)	12.4572(10)	10.9326(7)
α/°	90	90
β/°	95.943(3)	90
γ/°	90	90
V(Å^3)	324.26(4)	348.55(4)
Z	4	4
ρ(calcd)(g/cm^3)	5.311	5.837
Temp(K)	140(2)	140(2)
λ(Å)	0.71073	0.71073
F(000)	464.0	536.0
μ(mm^{-1})	16.948	14.987
R/wR($F_o^2 > 2\sigma(F_o^2)$)	0.0229/0.0562	0.0272/0.0633
R/wR(all data)	0.0233/0.0565	0.0274/0.0634
GOF on F^2	1.290	1.175
Flack parameter	N. A.	0.43(9)

$R(F) = \Sigma||F_o| - |F_c||/\Sigma|F_o|$. $wR(F_o^2) = [\Sigma w(F_o^2 - F_c^2)^2/\Sigma w(F_o^2)^2]^{1/2}$

Table S2. Atomic coordinates and equivalent isotropic displacement parameters (Å^2) for $ZnIO_3F$.

atom	x	y	z	U(eq)
I	0.01570(6)	0.68334(6)	0.33095(2)	0.00441(13)
Zn	0.52963(11)	0.24363(12)	0.43413(5)	0.00555(16)
F	0.7341(6)	-0.0777(6)	0.4748(2)	0.0085(6)
O1	0.1504(7)	0.5871(7)	0.2073(3)	0.0079(4)
O2	0.2830(7)	0.5667(7)	0.4295(3)	0.0079(4)
O3	-0.2125(7)	0.4169(7)	0.3335(3)	0.0079(4)

Table S3. Atomic coordinates (× 10^4)and equivalent isotropic displacement parameters (Å^2 × 10^3) for $CdIO_3F$.

atom	x	y	z	U(eq)
I	0.02495(10)	0.40186(9)	0.11608(4)	0.00581(16)

Cd	0.04472(12)	0.67952(11)	-0.14494(5)	0.00578(17)
F	-0.2433(11)	0.4352(10)	-0.2117(5)	0.0090(11)
O1	0.1819(13)	0.3507(12)	-0.0275(6)	0.0090(13)
O2	0.2679(13)	0.5439(11)	0.2026(6)	0.0066(13)
O3	-0.1228(12)	0.6611(12)	0.0527(6)	0.0080(12)

Table S4. Selected atomic distances (Å) for $ZnIO_3F$.

I–O3	1.803(4)	Zn–O1[b]	2.064(4)
I–O1	1.815(4)	Zn–O2	2.088(4)
I–O2	1.827(4)	Zn–O2[c]	2.097(4)
Zn–F	2.002(3)	Zn–O3[d]	2.097(4)
Zn–F[a]	2.025(3)		

Symmetry transformations used to generate equivalent atoms:

[a] 1-X, -Y, 1-Z [b] 1/2-X, -1/2+Y, 1/2-Z

[c] 1+X, Y, Z [d] 1/2-X, 1/2+Y, 1/2-Z

Table S5. Selected atomic distances (Å) for $CdIO_3F$.

I–O1	1.816(6)	Cd–O1	2.418(7)
I–O2	1.833(7)	Cd–O2[b]	2.299(7)
I–O3	1.843(7)	Cd–O2[c]	2.349(7)
Cd–F	2.247(6)	Cd–O3	2.352(6)
Cd–F[a]	2.285(7)	Cd–O3[d]	2.285(7)

Symmetry transformations used to generate equivalent atoms:

[a] -X, 1/2+Y, -1/2-Z [b] -1/2+X, 3/2-Y, -Z

[c] 1/2-X, 1+Y, -1/2-Z [d] 1/2+X, 3/2-Y, -Z

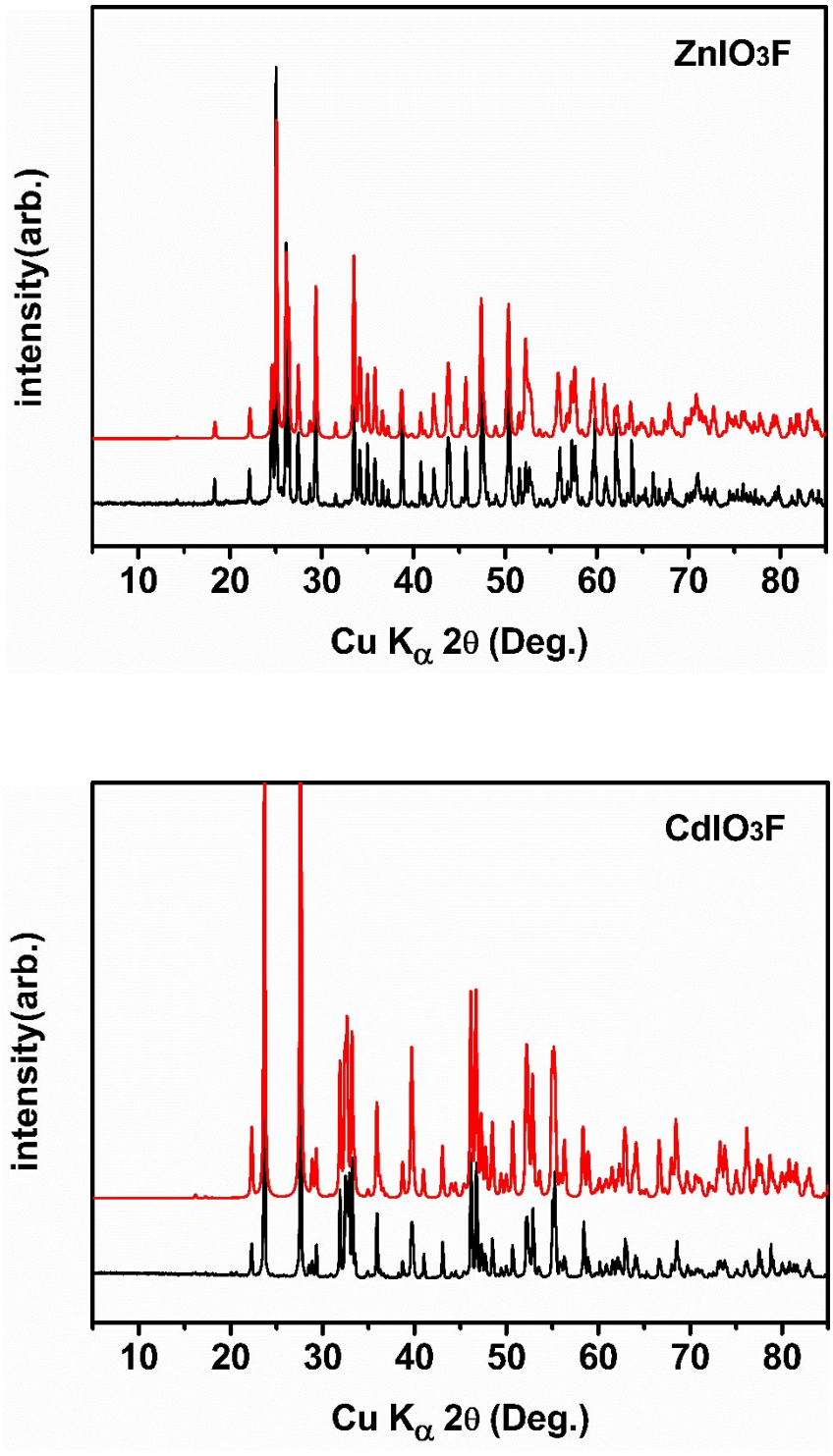

Figure S1. Experimental and calculated XRD patterns for MIO_3F (M = Zn, Cd). The red curves are the calculated ones, the black are patterns of samples.

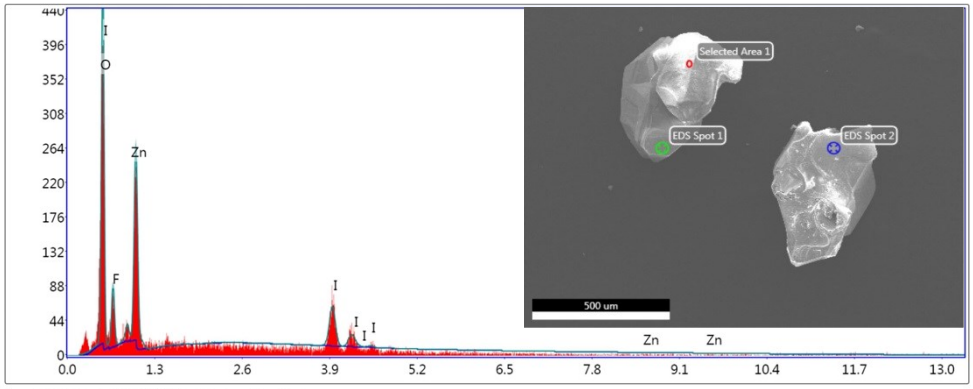

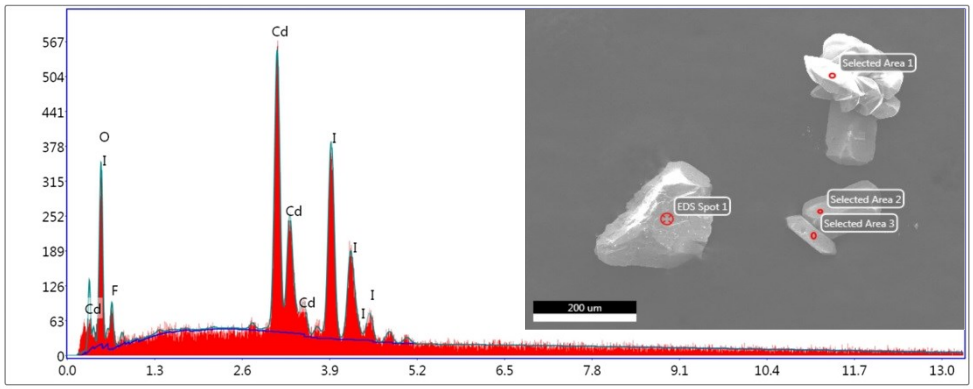

Figure S2. EDS analysis for MIO_3F (M = Zn, Cd). The inset is the SEM image of the tested crystal.

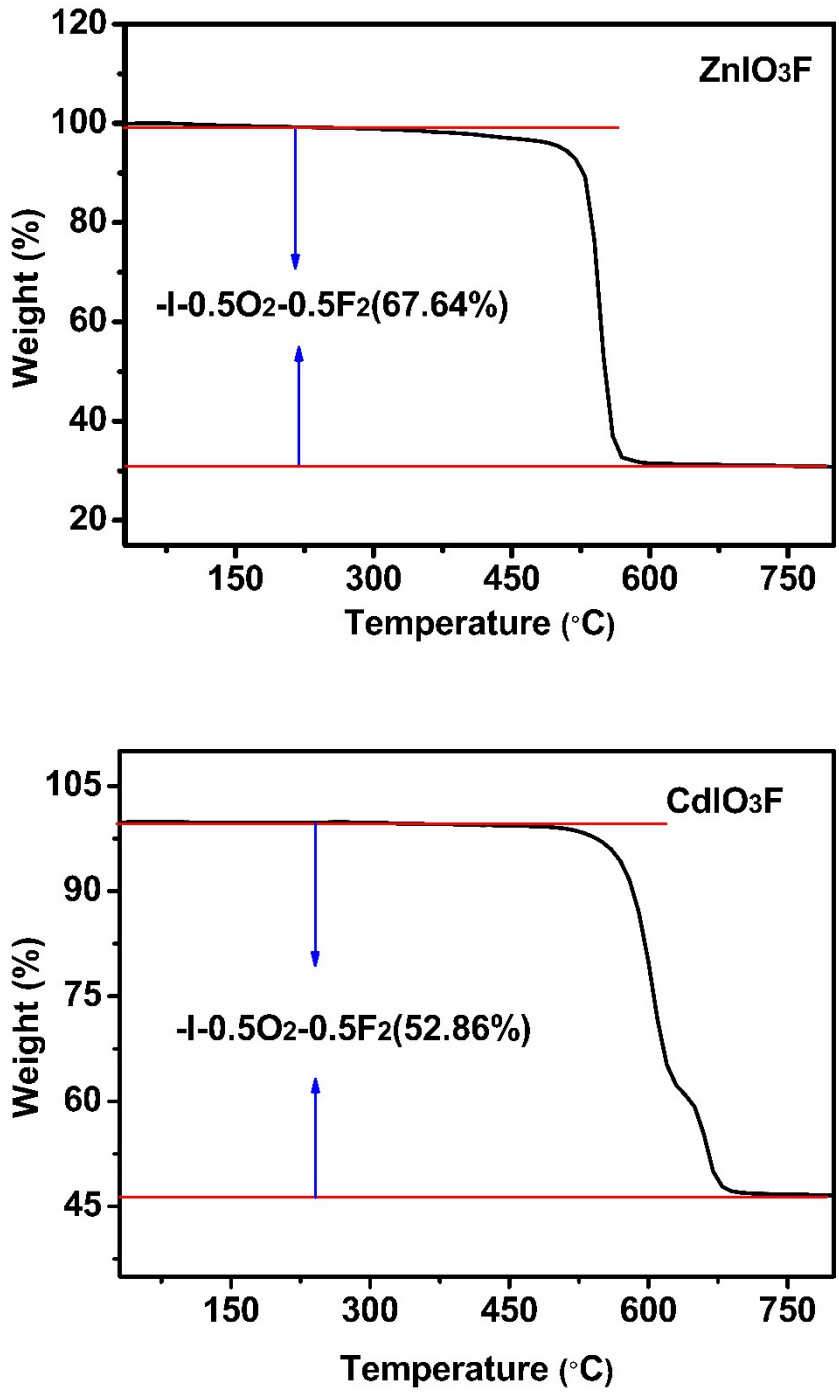

Figure S3. TG diagrams for MIO_3F (M = Zn, Cd).

$CdIO_3F$ has the highest thermostability among the known NCS iodate fluorides ,which could be attributed to the rigid structure of $CdIO_3F$ with following two points: (i) the weight losses of crystal with hydrogen-bearing groups (H_2O, OH^-, NH^{4+}, etc.) occurred in the lower temperature, such as, $Ce(IO_3)_2F_2 \cdot H_2O$ (178 °C) and $NH_4Bi_2(IO_3)_2F_5$ (270 °C). Thereby $CdIO_3F$ has structural advantages to avoid low thermal stability. (ii) there are two types of the structures of reported metal iodate fluorides without hydrogen-bearing groups, a) polyhedra centered on metal cations (m-centered polyhedra) are

interlinked into 1D chains, which further connect each other via the $[IO_3]^-$ groups to construct the 2D layered structure or 3D framework structure, however, as bridges between chains, bond energy of $[IO_3]^-$ groups are not strong enough. Therefore, the thermal stability of type-a metal iodate fluorides are not high, such as $ABi_2(IO_3)_2F_5$ (A = K, Rb and Cs) (240-270 ^oC), β-$Ba[VFO_2(IO_3)_2]$ (470 ^oC), α-/β-$Ba_2[VO_2F_2(IO_3)_2]IO_3$ (470 ^oC), $K_5(W_3O_9F_4)(IO_3)$ (250 ^oC) and $Sn(IO_3)_2F_2$ (400 ^oC); b) m-centered polyhedra connect with each other to form rigid 3D network with ring tunnels, which is conducive to the generation of high thermal stability, so $CdIO_3F$ exposses high thermal stability. However, type-b metal iodate fluorides $Bi(IO_3)F_2$ and $Bi_3OF_3(IO_3)_4$ are thermal stable up to 260 ^oC and 320 ^oC. For these three compounds, the rigidity of ring tunnels of $CdIO_3F$ and $Bi_3OF_3(IO_3)_4$ is significantly stronger than that of $Bi(IO_3)F_2$. Besides, the width of ring tunnel is 6.4194 Å (8.354 Å) and 12.933 Å (10.879 Å), respectively, but $CdIO_3F$'s is only 6.518 Å (7.004 Å). So $CdIO_3F$ is more stable than $Bi(IO_3)F_2$ and $Bi_3OF_3(IO_3)_4$ in structure.

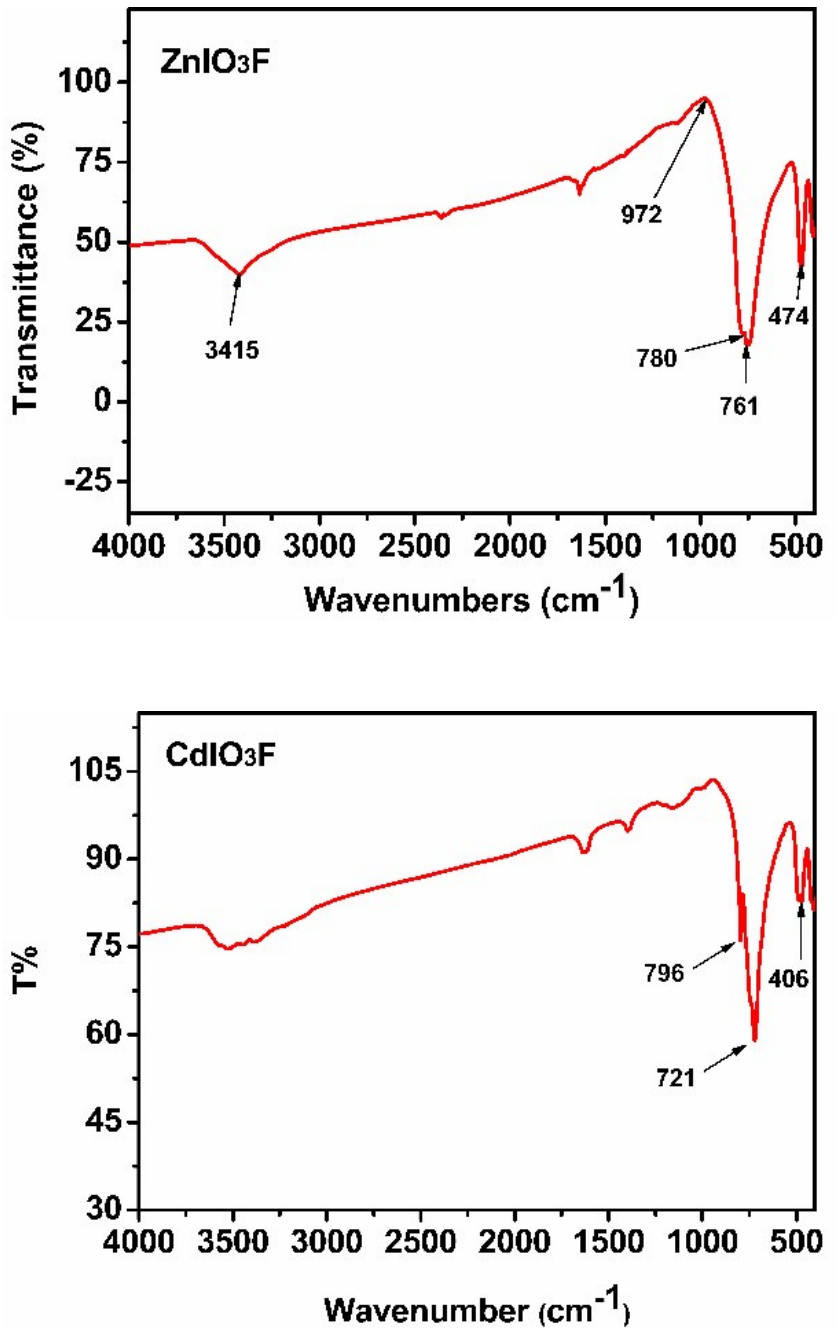

Figure S4 IR spectrum for MIO_3F (M = Zn, Cd).

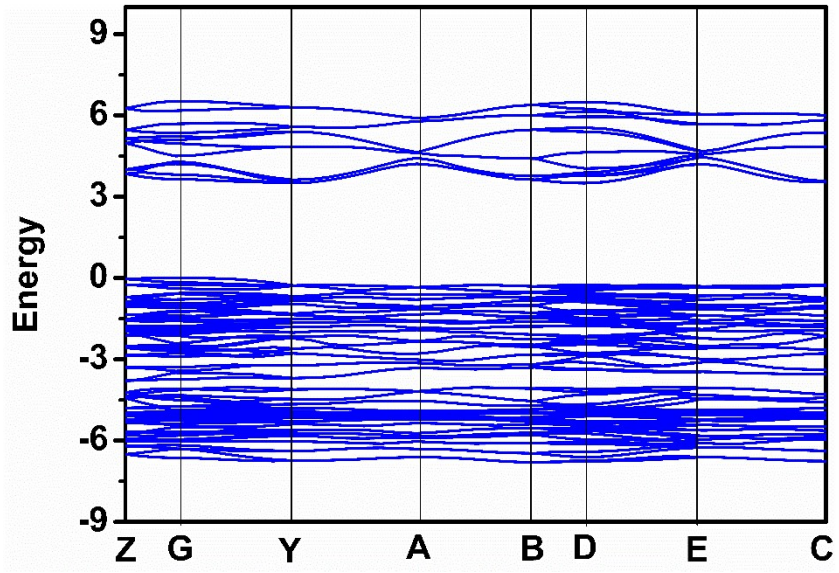

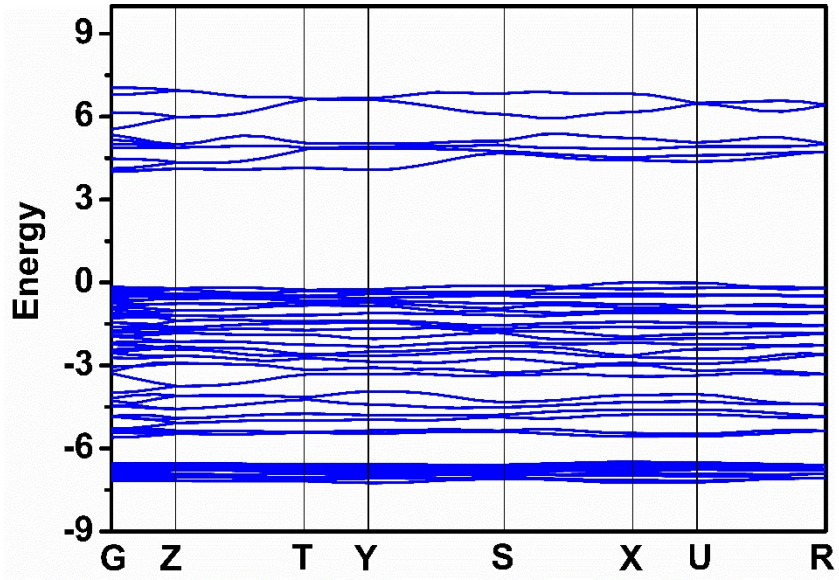

Figure S5. Band structure for MIO_3F (M = Zn, Cd).

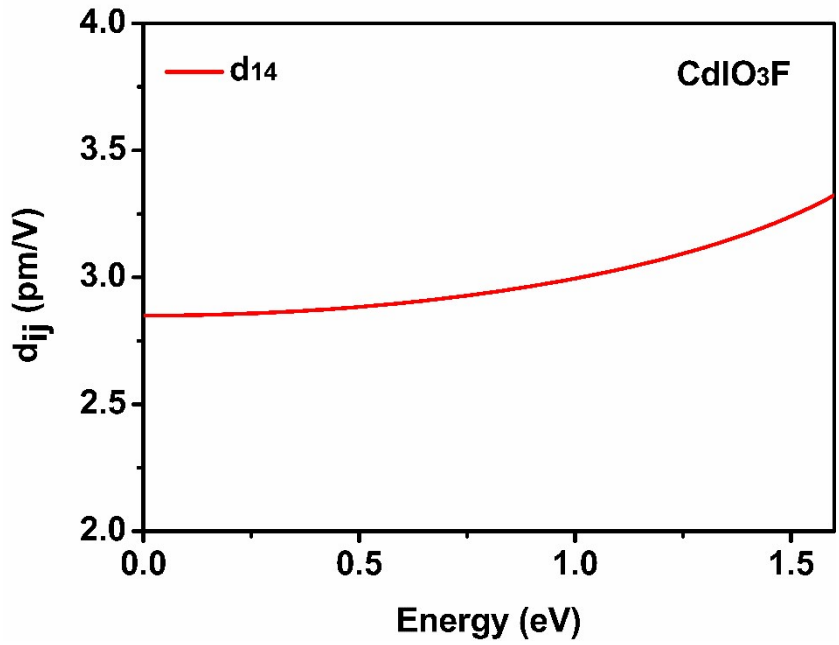

Figure S6. Calculated frequency-dependent second harmonic generation coefficients of $CdIO_3F$.

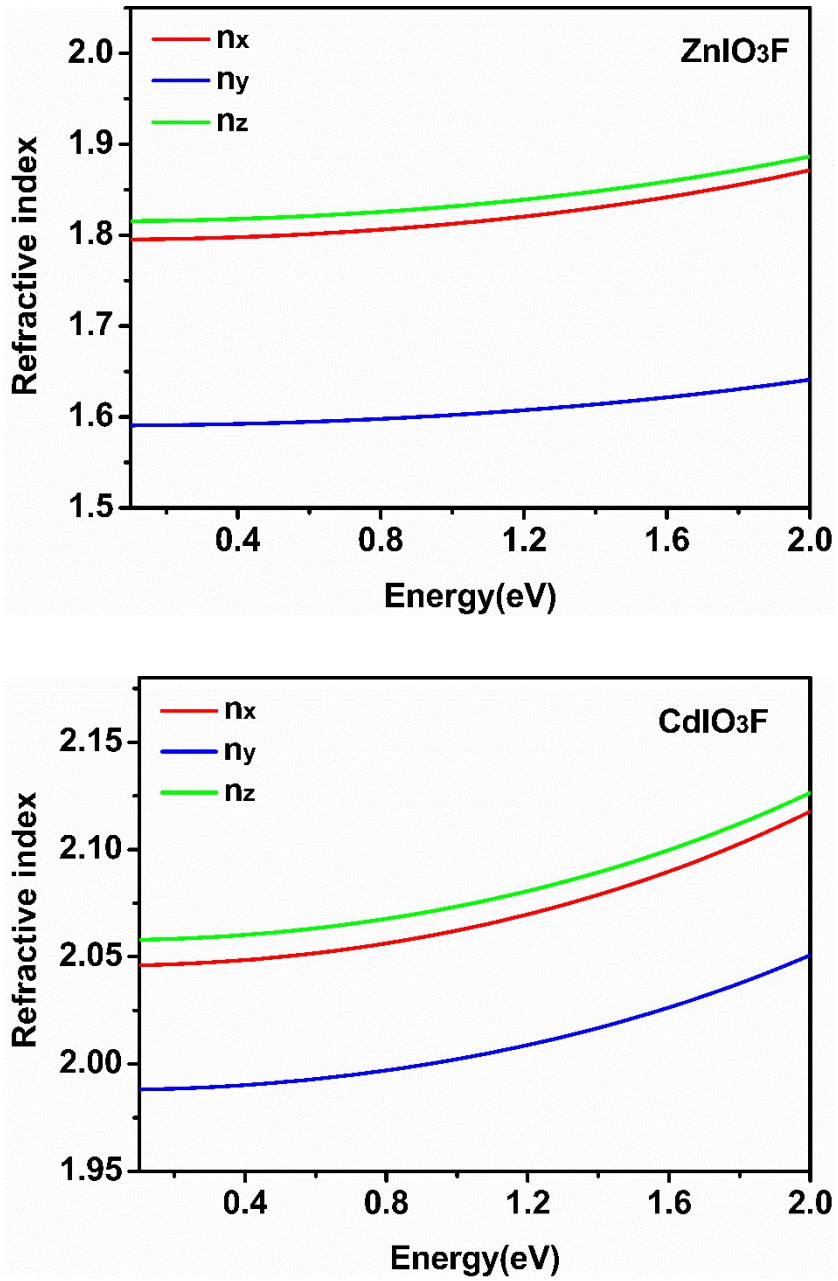

Figure S7. Calculated refractive index for MIO_3F (M = Zn, Cd).

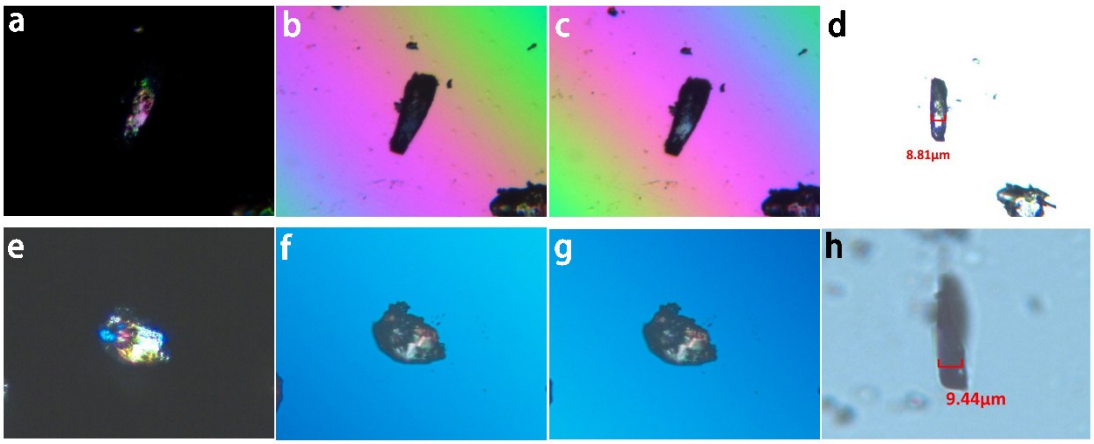

Figure S8. Photograph of $ZnIO_3F$ (a-d) and $CdIO_3F$ (e-h) for the measurement of birefringence.

Reference

1. J. Spooren, A. Rumplecker, A. F. Millange and R. I. W. , *Cheminform*, 2003, **34**, 1401-1403.
2. (a) G. M. Sheldrick, *Acta Crystallographica*, 2008, **64**, 112–122; (b) G. M. Sheldrick, *Acta Crystallogr C Struct Chem*, 2015, **71**, 3-8.
3. A. L. Spek, *J. Appl. Crystallogr.*, 2010, **36**, 7-13.
4. (a) P. Kubelka and F. Munk, 1931; (b) J. Tauc, *Mater. Res. Bull.*, 1970, **5**, 721.
5. S. K. Kurtz and T. T. Perry, *J. Appl. Phys.*, 1968, **39**, 3798.
6. M. C. Payne, M. P. Teter, D. C. Allan, T. A. Arias and J. D. Joannopoulos, *Rev. Mod. Phys.*, 1992, **64:4**, 1045-1097.
7. S. J. Clark, M. D. Segall, C. J. Pickard, P. J. Hasnip, M. I. J. Probert, K. Refson and M. C. Payne, *Zeitschrift Für Kristallographie*, 2005, **220**, 567-570.
8. J. P. Perdew, K. Burke and M. Ernzerhof, *Phys. Rev. Lett.*, 1996, **77**, 3865-3868.
9. L. Kleinman and D. M. Bylander, *Phys.rev.lett*, 1982, **48**, 1425.